

High-resolution magic angle spinning ^1H nuclear magnetic resonance spectroscopy metabolomics of hyperfunctioning parathyroid glands



Stéphanie Battini, PhD Student,^a Alessio Imperiale, MD, PhD,^{a,b,c} David Taïeb, MD, PhD,^d Karim Elbayed, PhD,^a A. Ercument Cicek, PhD,^{f,g} Frédéric Sebag, MD, PhD,^e Laurent Brunaud, MD, PhD,^h and Izzie-Jacques Namer, MD, PhD,^{a,b,c} Strasbourg, Marseille, and Nancy, France, Pittsburgh, PA, and Ankara, Turkey

Background. Primary hyperparathyroidism (PHPT) may be related to a single gland disease or multiglandular disease, which requires specific treatments. At present, an operation is the only curative treatment for PHPT. Currently, there are no biomarkers available to identify these 2 entities (single vs. multiple gland disease). The aims of the present study were to compare (1) the tissue metabolomics profiles between PHPT and renal hyperparathyroidism (secondary and tertiary) and (2) single gland disease with multiglandular disease in PHPT using metabolomics analysis.

Methods. The method used was ^1H high-resolution magic angle spinning nuclear magnetic resonance spectroscopy. Forty-three samples from 32 patients suffering from hyperparathyroidism were included in this study.

Results. Significant differences in the metabolomics profile were assessed according to PHPT and renal hyperparathyroidism. A bicomponent orthogonal partial least square-discriminant analysis showed a clear distinction between PHPT and renal hyperparathyroidism ($R^2Y = 0.85$, $Q^2 = 0.63$). Interestingly, the model also distinguished single gland disease from multiglandular disease ($R^2Y = 0.96$, $Q^2 = 0.55$). A network analysis was also performed using the Algorithm to Determine Expected Metabolite Level Alterations Using Mutual Information (ADEMA). Single gland disease was accurately predicted by ADEMA and was associated with higher levels of phosphorylcholine, choline, glycerophosphocholine, fumarate, succinate, lactate, glucose, glutamine, and ascorbate compared with multiglandular disease.

Conclusion. This study shows for the first time that ^1H high-resolution magic angle spinning nuclear magnetic resonance spectroscopy is a reliable and fast technique to distinguish single gland disease from multiglandular disease in patients with PHPT. The potential use of this method as an intraoperative tool requires specific further studies. (Surgery 2016;160:384-94.)

From the ICube,^a UMR 7357 University of Strasbourg/CNRS; Department of Biophysics and Nuclear Medicine,^b Hautepierre Hospital, University Hospitals of Strasbourg; and the FMTS, Faculty of Medicine,^c Strasbourg; La Timone University Hospital, European Center for Research in Medical Imaging^d and the Department of Endocrine Surgery,^e Aix-Marseille University, Marseille, France; Lane Center for Computational Biology, School of Computer Science,^f Carnegie Mellon University, Pittsburgh, PA; Computer Engineering Department,^g Bilkent University, Ankara, Turkey; and the Department of Digestive, Hepato-Biliary and Endocrine Surgery,^h Brabois University Hospital, Nancy, France

PRIMARY HYPERPARATHYROIDISM (PHPT) is the 3rd most common endocrine disorder after diabetes and hyperthyroidism. PHPT is classically associated with elevated total serum calcium (after

adjustment for albumin concentration) and elevated serum parathyroid hormone (PTH) level. In some cases, PTH levels may be normal but inappropriate to hypercalcemia.

L.B. and I.-J.N. contributed equally to this article.

The authors declare that there are no competing interests.

Accepted for publication March 7, 2016.

Reprint requests: Izzie-Jacques Namer, MD, PhD, Department of Biophysics and Nuclear Medicine, University Hospital of

Strasbourg, Hautepierre Hospital, Strasbourg Cedex, France.
E-mail: Izzie.Jacques.NAMER@chru-strasbourg.fr.

0039-6060/\$ - see front matter

© 2016 Elsevier Inc. All rights reserved.

<http://dx.doi.org/10.1016/j.surg.2016.03.002>

An operation is the only curative treatment for PHPT. According to recent recommendations,¹ an operation is indicated in any patient younger than 50, in any symptomatic patient, and in asymptomatic patients who meet some criteria. Although a single parathyroid adenoma (single gland disease [SGD]) is the most frequent occurrence, multiglandular disease (MGD) with multiple adenomas or multiglandular hyperplasia is present in 15–20% of cases. A conventional operation for PHPT relies on the inspection of the 4 parathyroid glands through bilateral cervical exploration. In recent years, a significant shift toward targeted operations has been proposed, relying on the accurate characterization of parathyroid glands (SGD versus MGD) by preoperative imaging.

However, first-line imaging studies show limited performance in the distinction between SGD and MGD (accuracy for predicting SGD is about 70–80%).² In order to further reduce the risk for operative failure, several institutions routinely use intraoperative PTH monitoring as an adjunct to determine the extent of the operation. However, intraoperative PTH monitoring does not have a consensual definition for prediction of operative cure and is still associated with the risk of unnecessary bilateral neck exploration.

Beyond a serum marker, better characterization of parathyroid tissue would be of particular interest in PHPT. Gross examination and intraoperative extemporaneous microscopic examination are unreliable. In recent years, metabolomics, or global metabolite profiling, has been used for investigating metabolite changes associated with some pathologic conditions (eg, colorectal cancers,³ breast cancers,⁴ liver cancers,⁵ and pancreatic cancers⁶).

Metabolomics represents the latest stage in the multi-omics approaches and is a growing-up technique behind genomics, transcriptomics, and proteomics, generating great interest in scientific and medical communities over the past few years. Starting from a broad analysis of small molecule metabolites, the metabolomics links cellular phenotype to its genotype and provides biochemical information related to the regulation of specific gene transcripts that are altered in the tumoral genome.⁷

Currently, well-recognized tools for metabolomics are nuclear magnetic resonance (NMR) spectroscopy and gas–mass spectrometry (GC-MS) or liquid chromatography–mass spectrometry (LC-MS). GC-MS and LC-MS are more widely represented in the technical platforms related to metabolomics, mainly because they demonstrate a better sensitivity than does NMR spectroscopy.

However, these technologies generate massive amounts of data that are often difficult to interpret or to use for building predictive models.

However, among NMR techniques, ¹H high-resolution magic angle spinning (HRMAS) NMR spectroscopy is especially suited to analyzing a small volume of intact tissue samples and avoiding any chemical extraction procedures or sample manipulation, which are necessary for both MS and liquid-state NMR or well-established immunohistochemistry. HRMAS NMR spectroscopy enables identification and quantification of several metabolites from spectra with excellent resolution and signal-to-noise ratio. Recently, we and other groups have proved that metabolomics is a promising tool in the characterization of some endocrine tumors such as pheochromocytomas/paragangliomas.^{8,9}

Consequently, there is a need for accurate biomarkers that could help surgeons to distinguish between SGD and MGD. The aims of the present study were (1) to evaluate if metabolomics patterns were different between PHPT and renal hyperparathyroidism (secondary and tertiary) and (2) to compare the metabolomic profiles of SGD and MGD in PHPT patients, using metabolomics analysis.

MATERIALS AND METHODS

Patient population. Forty-three tissue samples of sporadic hyperfunctioning parathyroid tissue were analyzed and retrospectively selected from 32 patients (Fig 1) suffering from hyperparathyroidism and operated on between January 2013 and November 2014 in 2 academic endocrine tumor centers (Brabois University Hospital, Nancy, France, and La Timone University Hospital, Marseille, France). Only patients who fulfilled the following criteria were included: (1) diagnosis of hyperparathyroidism (primary versus secondary [SHPT] versus tertiary [THPT]), (2) 6-month follow-up after parathyroidectomy for PHPT in order to distinguish SGD from MGD, (3) absence of personal history of therapeutic radiation, and (4) parathyroid glands collected just after resection and snap-frozen in liquid nitrogen before storage.

A written informed consent was obtained from all the included patients. For this investigation, the tissue samples were obtained from the tumor biobank of Nancy (n° BB-0033-00035) and Marseille University Hospitals (AP-HM tissue bank AC 2013-1786).

Disease status. For PHPT, SGD was defined when only a single abnormal gland was removed

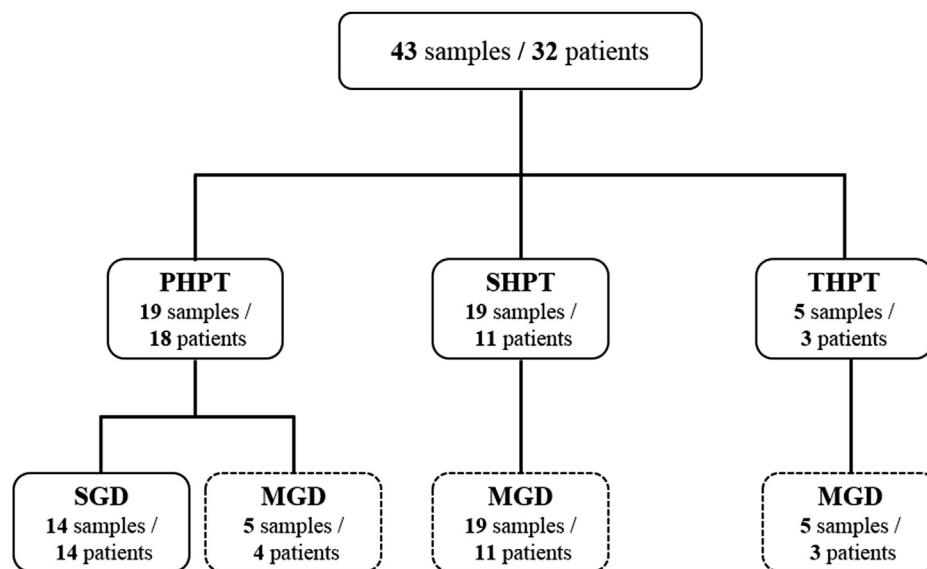


Fig 1. Studied patient population and examined hyperfunctioning parathyroid samples.

and the patient was cured (normalization of serum calcium for ≥ 6 months following parathyroidectomy). When >1 gland was involved histologically (adenoma or hyperplasia), the patient was considered to have MGD, including cases of multiple gland parathyroid hyperplasia. All patients were cured at 6 months postoperatively. Patient and tumor characteristics are detailed in Table I.

Tissue sample preparation for HRMAS NMR spectroscopy. All tissue specimens were collected during the operation just after tumor removal and were snap-frozen in liquid nitrogen until the sample preparation for the HRMAS NMR analysis. The amount of tissue used for HRMAS analysis ranged from 6–20 mg. Each tissue sample was placed in a 30 μL disposable insert. Next, 8 μL of deuterium oxide with 0.75 weight percent 2,2,3,3-D₄-3-(trimethylsilyl) propionic acid were added to every biopsy's insert in order to get a chemical shift reference for the NMR spectrometer.

The exact weight of the sample used was determined by weighing the empty insert and the insert containing the tissue sample. Then, inserts were kept at -80°C until the HRMAS NMR analysis was performed. The insert was stored at -80°C and placed in a 4-mm ZrO₂ rotor just before the HRMAS NMR analysis. The percentage of parathyroid cells in each analyzed sample was estimated on frozen sections using a mirror sample. All examined samples contained $\geq 80\%$ parathyroid cells.

HRMAS NMR data acquisition, spectra processing, and metabolite quantification. All HRMAS NMR spectra were achieved on an Avance

spectrometer (Bruker Avance III 500; Bruker Corporation, Billerica, MA; installed in the Pathological Department of Strasbourg University Hospitals) operating at a proton frequency of 500.13 MHz and equipped with a 4-mm double resonance gradient HRMAS probe (¹H and ¹³C). The temperature was maintained at 277.15 K throughout the acquisition time in order to reduce the effects of tissue degradation during the spectra acquisition.

A 1-dimensional (1D) proton spectrum using a Carr-Purcell-Meiboom-Gill (CPMG) pulse sequence and 1,024 transients was acquired for each serum sample.¹⁰ Free induction decays were multiplied by an exponential window function of 0.3 Hz prior to Fourier transformation and were corrected for phase and baseline distortions using TopSpin 3.2 (Bruker GmbH, Bremen, Germany). The chemical shift was calibrated to the peak of the methyl proton of L-lactate at 1.33 parts per million (ppm).

In order to confirm resonance assignments, 2-dimensional (2D) heteronuclear experiments were also recorded immediately after the end of the 1D spectra acquisition. Because the duration of these experiments is long and significant tissue degradation occurs during NMR acquisition, only a few representative samples were analyzed by 2D experiments. Each peak in the 2D spectra represents a correlation ¹H–¹³C. Spectra were referenced by setting the lactate doublet chemical shift to 1.33 ppm in proton dimension and 22.70 ppm in carbon dimension. Metabolites were assigned using a standard metabolite

Table I. Characteristics of 43 samples from 32 patients suffering from hyperparathyroidism

Patients	Sex	Age (y)	Parathyroid disorder	Localization	Mass (g)
1	M	54	PHPT-SGD	Left P3	0.080
2	M	62	PHPT-SGD	Right P3	1.350
3	F	56	PHPT-SGD	Left P4	1.390
4	F	76	PHPT-SGD	Left P4	NA
5	F	61	PHPT-SGD	Right P4	0.250
6	F	66	PHPT-SGD	Right P3	2.230
7	F	59	PHPT-SGD	Left P4	NA
8	F	55	PHPT-SGD	Right P4	3.400
9	F	55	PHPT-SGD	Right P4	0.600
10	F	65	PHPT-SGD	Left P3	NA
11	F	71	PHPT-SGD	Left P3	0.320
12	F	66	PHPT-SGD	Left P4	1.880
13	F	67	PHPT-SGD	Right P3	NA
14	F	57	PHPT-SGD	Left P3	9.600
15	M	77	PHPT-MGD	Left P4	3.800
16	F	78	PHPT-MGD	Left P4	NA
17	F	79	PHPT-MGD	Left P3	NA
18	F	67	PHPT-MGD	Right P4	1.000
				Left P4	NA
19	F	40	SHPT-MGD	Right P4	0.125
				Left P3	0.316
				Left P4	0.282
20	M	59	SHPT-MGD	Right P3	0.700
				Left P3	0.650
21	M	56	SHPT-MGD	Right P4	0.690
				Right P3	0.150
				Left P3	0.230
22	M	45	SHPT-MGD	Left P3	NA
23	M	37	SHPT-MGD	Right P3	NA
				Right P4	NA
24	M	32	SHPT-MGD	Left P3	NA
25	M	54	SHPT-MGD	Right P3	0.722
26	M	30	SHPT-MGD	Right P3	NA
				Left P4	NA
27	F	70	SHPT-MGD	Right P3	0.840
				Left P4	0.660
28	F	39	SHPT-MGD	Right P4	NA
29	F	58	SHPT-MGD	Right P3	0.200
30	F	62	THPT-MGD	Left P4	0.063
				Right P4	0.780
31	M	56	THPT-MGD	Left P3	1.400
				Left P4	0.150
32	F	60	THPT-MGD	Right P4	0.200

M, Male; F, female; PHPT, primary hyperparathyroidism; SHPT, secondary hyperparathyroidism; THPT, tertiary hyperparathyroidism; SGD, single gland disease; MGD, multiglandular disease; P3, inferior parathyroid gland; P4, superior parathyroid glands; NA, not available.

chemical shift table (Table II) available in the literature.¹¹ HRMAS NMR data acquisition and processing have been previously detailed.¹⁰

Metabolite quantification was performed using an external reference standard of lactate (3 μ moles), scanned under the same analytical

conditions. Spectra were normalized according to sample weight. Peaks of interest were automatically defined by an in-house program using MATLAB (MATLAB 7.0; MathWorks, Natick, MA). Peak integration was then compared with the one obtained with the lactate reference and was corrected according to the number of protons. Only well-defined peaks with no overlapping in the 1D CPMG spectra were selected for quantification. Quantification results were expressed as nmol/mg of tissue.

Statistical analysis. The region between 6.54 and 2.32 ppm of each 1D HRMAS NMR spectrum was automatically bucketed into integral regions of 0.01 ppm using AMIX software (AMIX 3.9.14; Bruker GmbH) to reduce the peak shift effect due to pH variations. This procedure generated an X-data matrix with 421 columns (buckets) and 43 rows corresponding to the 43 examined samples of hyperfunctioning parathyroid tissue. In this matrix, each point represents the center of a single bucket of 0.01 ppm in the NMR spectrum. Afterward, the data set was exported and analyzed in SIMCA P (version 13.0.3; Umetrics AB, Umeå, Sweden). The detailed procedure has been previously reported by our team.¹⁰

A combination of principal component analysis (PCA) and orthogonal partial least squares-discriminant analysis (OPLS-DA) was performed to analyze the data matrix.^{12,13} First, a PCA was performed to evaluate the quality of the data and to identify possible outliers. Then an OPLS-DA was employed to optimize the separation between groups and to classify the samples in each model. The following OPLS-DA models were considered: (a) PHPT versus renal HPT and (b) SGD versus MGD in PHPT. OPLS-DA was performed on the whole set of variables (spectral interval of 0.01 ppm) to select those with real discriminating power.¹⁴

Variables corresponding to variable importance for projection (VIP) value ≥ 1 were selected, allowing the selection of the following metabolites: fumarate, phosphorylcholine, glycerophosphocholine, choline, lactate, creatine, aspartate, GSH, glutamine, glutamate, ascorbate, succinate, β -glucose, taurine, scyllo-inositol, and myo-inositol. Cross-validation was used in each OPLS-DA model to determine the number of components and to avoid data overfitting.¹⁵ Two measurements of model quality were reported for OPLS-DA: R^2Y and Q^2 representing, respectively, the accuracy of fit (ie, data variation) and the accuracy of prediction, as estimated by cross-validation. $Q^2 \geq 0.5$ can be considered a good predictor.¹⁶

Table II. ^1H NMR resonance assignments of the metabolites identified in examined samples of hyperfunctioning parathyroid tissue

	<i>Metabolites</i>	<i>Groups</i>	^1H chemical shift (ppm)	^{13}C chemical shift (ppm)
1	Leucine	βCH_2	1.71	42.50
		$\alpha\text{CH-NH}_2$	3.73	56.1
		δCH_3	0.95	23.43
		$\delta'\text{CH}_3$	0.95	24.75
2	Valine	γCH_3	0.98	19.18
		$\gamma'\text{CH}_3$	1.04	20.66
		$\alpha\text{CH-NH}_2$	3.59	63.10
		βCH	2.30	32.0
3	Alanine	βCH_3	1.47	18.86
		αCH	3.78	53.26
4	Lysine	γCH_2	1.43	24.52
		$\gamma'\text{CH}_2$	1.50	24.18
		δCH_2	1.70	29.16
		βCH_2	1.90	32.60
		ϵCH_2	3.00	41.92
		γCH_2	1.91	30.25
5	Arginine	βCH_2	3.23	43.15
		$\epsilon\text{CH-NH}_2$	3.76	57.17
		γCH_2	1.70	26.64
		$\text{CH}_2\text{-CONH}$	2.55	33.96
6	Glutathione	$\text{CH}_2\text{-SH}$	2.95	28.33
		CH-NH_2	3.78	46.04
		CH	4.58	58.44
		CH_3	1.33	22.69
7	Lactate	CH	4.12	71.17
		C5H	3.27	77.02
8	Myo-Inositol	C1H, C3H	3.53	73.84
		C4H, C6H	3.61	75.05
		C2H	4.05	74.93
		CH_3	3.03	39.56
9	Creatine	CH_2	3.93	56.35
		$-\text{CH}_2\text{-NH}_3^+$	3.26	50.22
10	Taurine	$-\text{CH}_2\text{-SO}_3^-$	3.41	38.08
		CH-OH	3.60	73.96
11	Glycogen	CH-OH	3.78	63.30
		CH-OH	5.43	102.00
		βCH_2	2.06	29.76
12	Glutamic acid	γCH_2	2.34	35.97
		αCH	3.76	55.17
		βCH_2	2.16	28.90
13	Glutamine	γCH_2	2.44	33.50
		αCH_2	3.77	57.19
		$-\text{N}^+(\text{CH}_3)_3$	3.21	56.49
14	Choline	βCH_2	3.52	69.98
		αCH	4.06	58.36
		βCH_2	3.61	68.90
15	Phosphorylcholine	αCH	4.18	60.81
		$-\text{CH}_2\text{-NH}_3^+$	3.21	56.51
16	Glycerophosphocholine	βCH_2	3.69	68.47
		αCH_2	4.33	62.13
		CH_2OH	3.91	73.29
		$\text{CH}_2\text{-HPO}_4(\text{d})$	3.87	69.20
		$\text{CH}_2\text{-HPO}_4(\text{u})$	3.94	69.20

(continued)

Table II. (continued)

	Metabolites	Groups	^1H chemical shift (ppm)	^{13}C chemical shift (ppm)
17	Ascorbic acid	-CH-OH	4.02	72.16
		C ₄ H	4.53	80.89
18	Succinic acid	(α,β CH ₂)	2.39	34.0

Each peak in the 2D spectrum represents a correlation ^1H - ^{13}C .

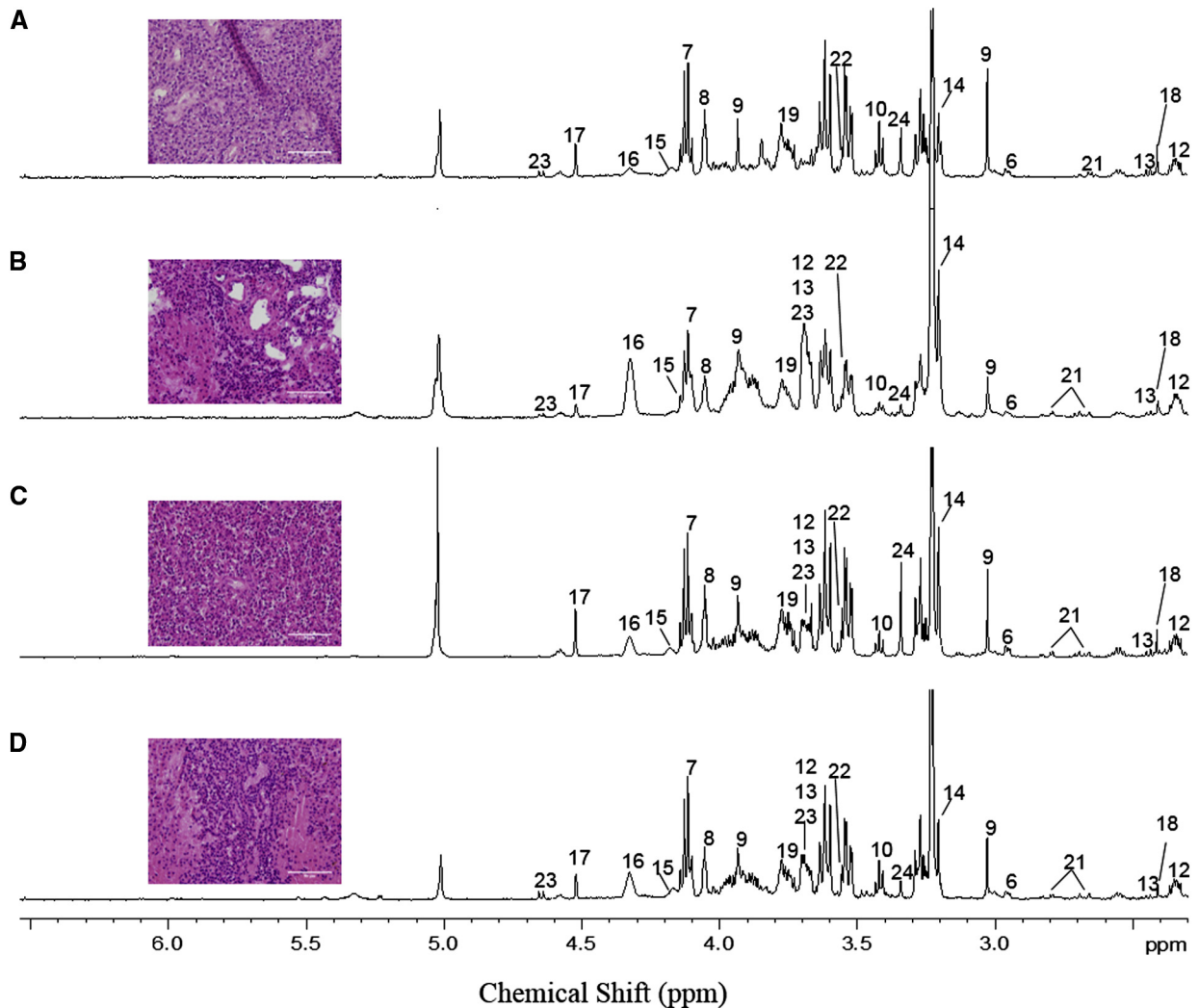


Fig 2. 1D ^1H HRMAS NMR spectra obtained from the analysis of hyperfunctioning parathyroid samples. (A) Primary parathyroid SGD; (B) primary parathyroid MGD; (C) secondary parathyroid MGD; (D) tertiary parathyroid MGD. The spectra metabolic contents are directly comparable, because the intensity of each spectrum has been normalized in respect to the weight of the analyzed sample. For display purposes, the amplitude of the lactate peak at 4.09 ppm and the glycerophosphocholine at 3.21 ppm have been graphically reduced. Metabolite assignments are given in Table I. Histologic features of hyperfunctioning parathyroid glands corresponding to each spectrum are depicted at the left side of the figure (HE \times 400; scale bars, 50 μm). (Color version of this figure is available online.)

Network analysis. The Algorithm to Determine Expected Metabolite Level Alterations Using Mutual Information (ADEMA) has been applied on metabolite quantification values. ADEMA evaluates the changes in groups of metabolites,

between the case and the control, instead of analyzing metabolites one by one.¹⁷ ADEMA includes the metabolic network topology and uses mutual information to find out if those metabolites are biomarkers when considered together

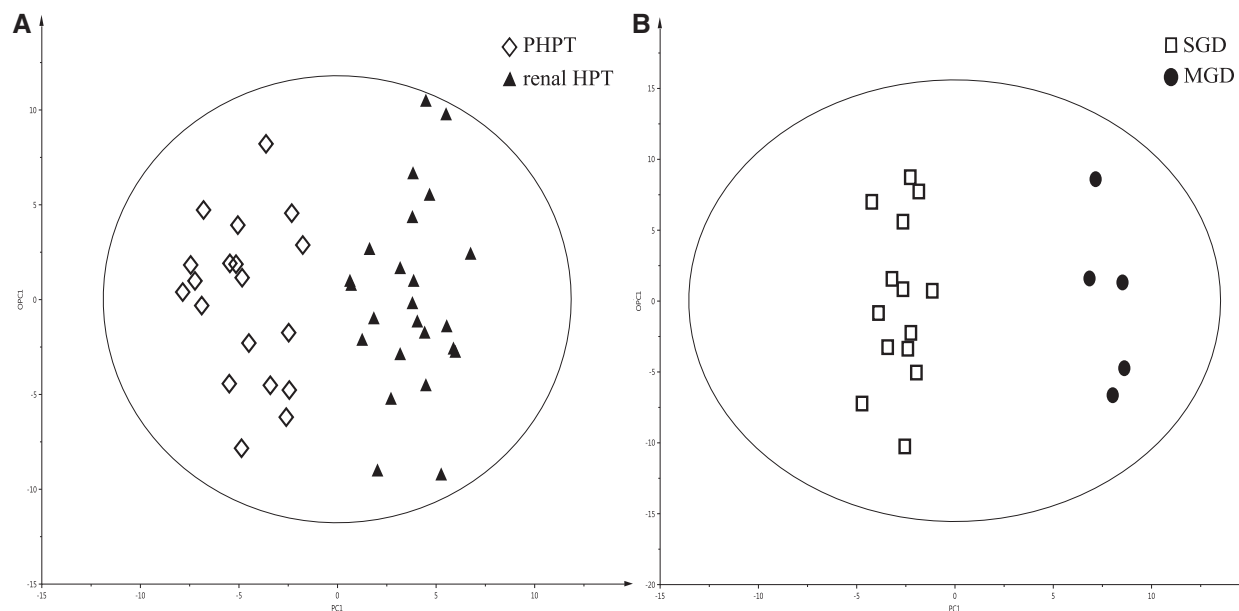


Fig 3. Results of bicomponent OPLS-DA models based on VIP metabolites: (A) Two-class model including 43 samples obtained with PHPT (19 samples) and 24 samples from patients with renal HPT and (B) two-class model including 14 and 5 samples of SGD and MGD from patients with PHPT. A clear distinction between the different classes of tissues is shown in both models.

and can predict the expected change's direction per metabolite, when metabolic network topology is considered. The network was constructed using Kyoto Encyclopedia of Genes and Genomes^{18,19} and Selway's work.²⁰

In order to compare the patients suffering from PHPT and SHPT/THPT and the patients suffering from SGD and MGD in the context of PHPT, the following groups of metabolites were defined: (1) Choline, Phosphorylcholine, Glycerophosphocholine, Total Choline; (2) Glutamine, Glutamate; (3) Glucose, Alanine, Lactate; (4) Succinate, Fumarate; (5) Glutathione, Glutamate; and (6) Glutathione, Ascorbate.

For discretization of metabolite observations, we have set a number of levels (M) as 6 and a number of levels that can be assigned to observation (k) as 4. Using the above mentioned metabolite groups and parameters, an expected metabolite level for the case and for the control is obtained per metabolite. The direction of the expected change is obtained by comparing expected levels.

RESULTS

Tissue samples. Accordingly, 19 samples were obtained from 18 patients with PHPT, 19 samples from 11 patients with SHPT, and 5 samples from 3 patients suffering from THPT. Among the 19 samples obtained from patients with PHPT, 14 were classified as SGD, while the 5 others had

MGD (all were described as hyperplastic glands by the pathologist; Fig 1). All patients were cured at 6 months postoperatively.

Spectra quality. All the spectra obtained from the 43 analyzed specimens were of high quality without any signs of tissue necrosis. The spectral region within the range of 2.32–0 ppm has been voluntarily excluded from the analysis because of important signal overlapping related to high and complex fatty acids signals. The representative 1D HRMAS NMR CPMG spectrum for each analyzed sample class is shown in Fig 2. A total of 25 metabolites were identified within the range of 6.54–2.32 ppm from the spectra obtained from all 43 tissue samples. The spectra obtained from different glands within the same patient show similar profiles.

PHPT versus renal HPT. OPLS-DA results. Forty-three samples were studied in this 2-class model. Nineteen samples were obtained from patients with PHPT and 24 from patients with renal HPT (11 patients/19 samples of SHPT and 3 patients/5 samples of THPT). PCA was first applied to our data (43 HPT), showing a homogeneous population without any outliers. The 2 classes were clearly separated by a bi-component OPLS-DA based on the VIP metabolites. (The VIP value is namely a weighted sum of squares of the PLS weights, which takes into account the explained variance of each OPLS dimension.)

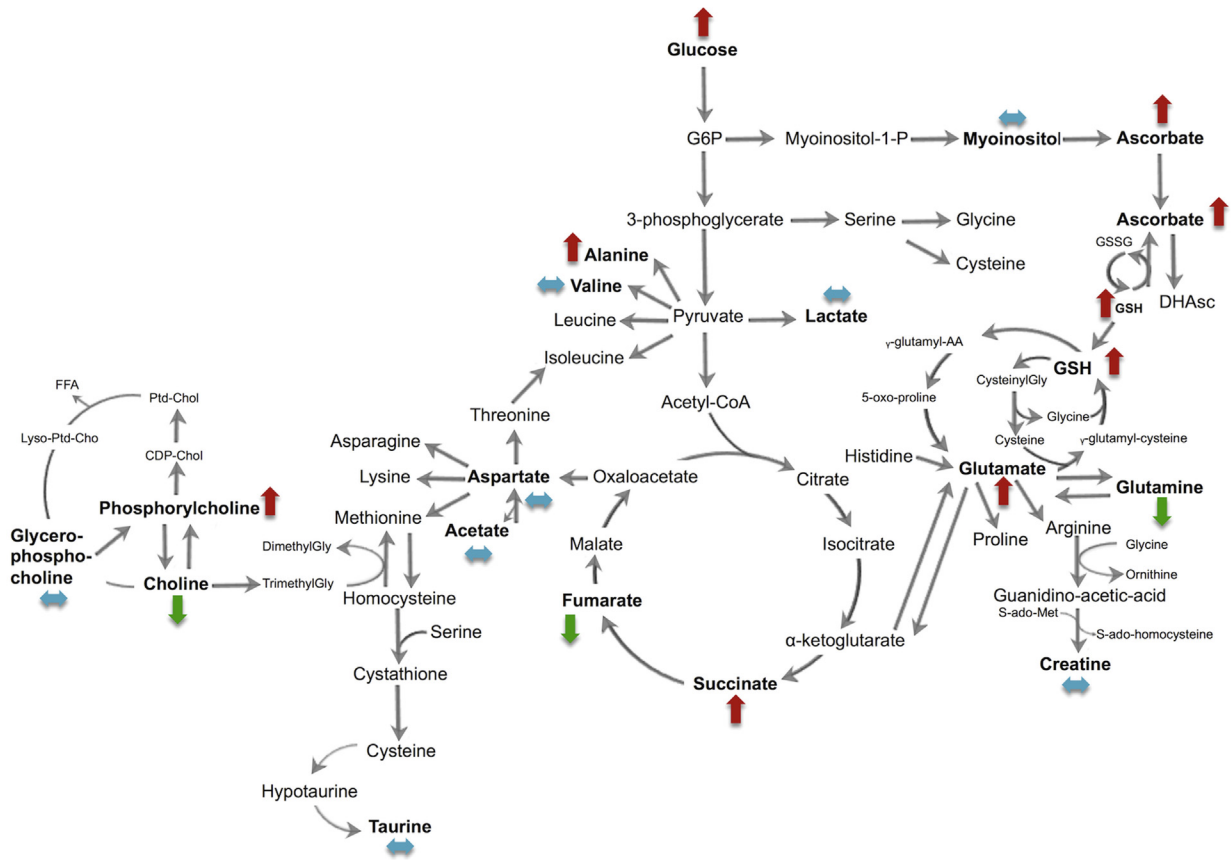


Fig 4. Metabolic network analysis according to ADEMA results comparing PHPT-related samples (19 samples) to renal HPT-related samples (24 samples). The red, green, and blue arrows, respectively, indicate the metabolites that are predicted to increase, decrease, and remain stable between the 2 groups.

The VIP values were employed to identify the features contributing to group separation (Fig 3, A), showing an accurate representation of the data and good cumulative confidence criterion of fit ($R^2Y = 0.85$) and prediction ($Q^2 = 0.63$). A higher level of β -glucose, ascorbate, phosphorylcholine, taurine, GSH, myo-inositol, and glutamate was revealed in patients with PHPT. On the contrary, a higher concentration of fumarate, choline, serine, glycerophosphocholine, aspartate, and glutamine was shown in patients with renal HPT.

Network analysis. When the data were analyzed using the ADEMA algorithm and the metabolic subnetwork depicted in Fig 4, a higher level of phosphorylcholine, succinate, alanine, glucose, ascorbate, GSH, and glutamate was predicted in PHPT. Moreover, a decreased level of choline, fumarate, and glutamine was predicted in PHPT. Finally, glycerophosphocholine, taurine, acetate, aspartate, valine, lactate, myo-inositol, and creatine were predicted to be equivalent between the 2 groups.

SGD versus MGD in PHPT. OPLS-DA results. Fourteen SGD were secondly compared to 5 samples of MGD. No outliers were evident at PCA analysis. The 2nd population was homogeneous, too. A bicomponent OPLS-DA analysis based on VIP metabolites (Fig 3, B) clearly separated the 2 classes of analyzed tissues ($R^2Y = 0.96$, $Q^2 = 0.55$), revealing a higher concentration of fumarate, β -glucose, ascorbate, myo-inositol, glycine, scyllo-inositol, and choline in SGD samples. On the other hand, SGD revealed a higher level of glutamate, glutamine, lactate, taurine, GSH, and aspartate compared with MGD.

Network analysis. Using the ADEMA algorithm, the metabolic subnetwork included a higher level of phosphorylcholine, choline, glycerophosphocholine, fumarate, succinate, lactate, glucose, glutamine, and ascorbate predicted in SGD (Fig 5). Moreover, the model accurately predicted a decreased level of alanine, glutamate, and GSH in MGD. Finally, taurine, acetate, aspartate, valine,

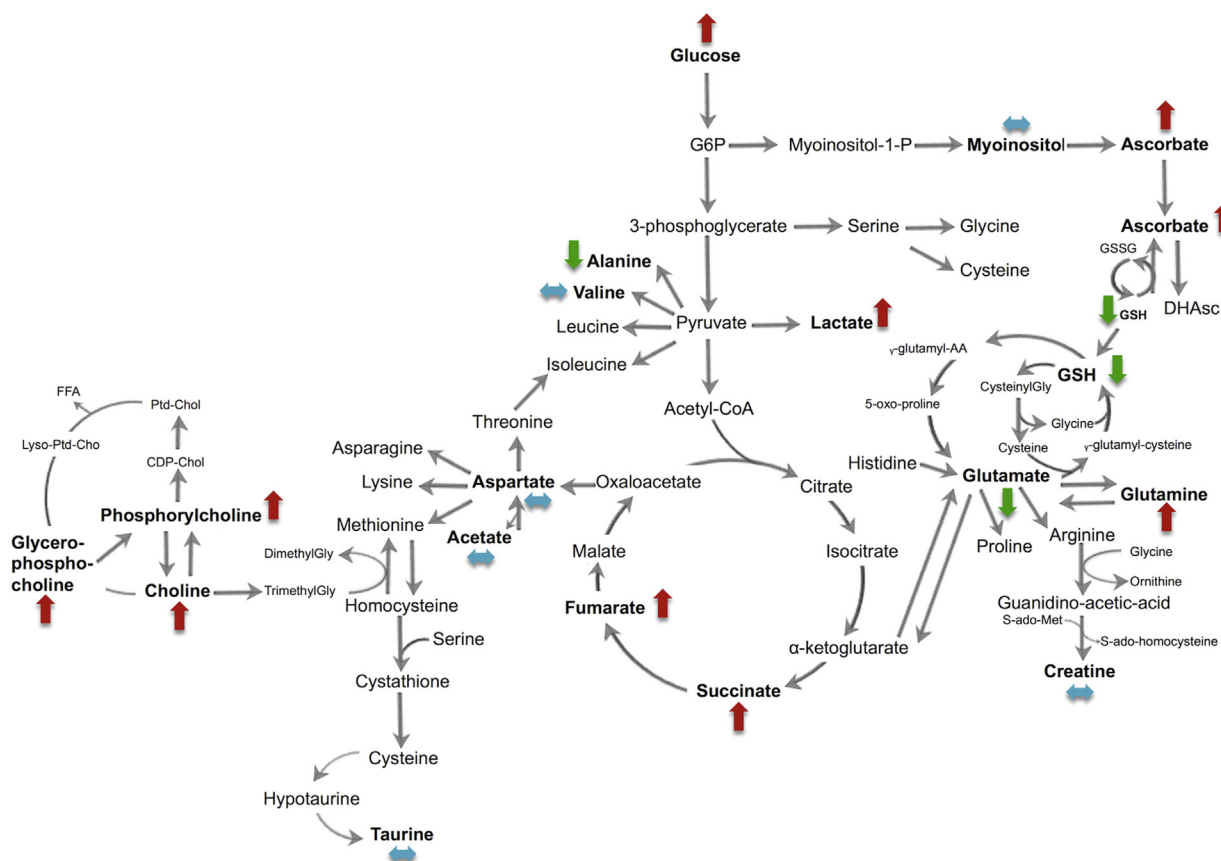


Fig 5. Metabolic network analysis according to ADEMA results, comparing PHPT-related SGD (14 samples) and MGD (5 samples). The red, green, and blue arrows respectively indicate the metabolites that are predicted to increase, decrease, and remain stable between the 2 groups.

myo-inositol, and creatine were predicted to be equivalent between SGD and MGD.

DISCUSSION

To the best of our knowledge, this is the first study that has evaluated the metabolome of hyperfunctioning parathyroid glands in the context of parathyroid hyperfunctioning disorders. The principal conclusions that can be drawn from this preliminary study include: (1) There are differences between PHPT and renal HPT from a metabolomic standpoint. (2) SGD and MGD can be distinguished by metabolomic profiling and can be accurately predicted by our model. (3) This approach provides new insights into the relationships between metabolic pathways and parathyroid disorders.

It is widely accepted that bilateral parathyroid exploration is no longer the only option for patients with PHPT, and those with an SGD in imaging studies can also be candidates for focused approaches. Parathyroid scintigraphy (PS) and

parathyroid ultrasonography (US) are the preferred approaches reported by endocrine surgeons for selecting candidates for a focused approach.^{21,22} The Positive Predictive Value for an SGD in cases of concordant results between US and PS for a single gland abnormality is about 90%. In order to reduce the risk of failure, many institutions use intraoperative PTH (IOPTH) monitoring.²³

According to the Miami criteria,²⁴ a 50% decrease in PTH levels 10 minutes after removal of the putative lesion suggests a curative operation. However, the assay might sometimes yield inaccurate results,²⁵⁻²⁸ as when PTH concentrations may decrease even in the presence of MGD. IOPTH monitoring might also wrongly lead to a bilateral operation. Finally, one of the main drawbacks of IOPTH is that its accuracy is widely dependent on preoperative PTH levels, gland sizes, and parathyroid tissues' sensitivity to serum calcium.

Beyond IOPTH, the use of a more specific marker tightly linked to the pathophysiology of the parathyroid disease would be of particular

interest. Because HRMAS NMR spectroscopy enables rapid characterization of intact tissue, it could also be used as an intraoperative method. In our hospital, intraoperative real-time analysis is performed for gliomas in neurosurgery ("ExtempoNMR" project). Fast transportation of samples is performed by a pneumatic tube system.

Sample preparation is quick and easy; it does not take more than 2 minutes to prepare snap-frozen biopsy and inclusion within an insert of a 20-mg parathyroid tissue sample. HRMAS analysis takes 10 minutes for settings and an additional 10 minutes for spectrum acquisition. Data analysis is also very quick (<10 minutes). If confirmed, this approach could be used in clinical routine for classification of SGD versus MGD and could even coexist with IOPTH. Furthermore, the cost is <\$50 per sample.

Based on our preliminary results, we expect that metabolomic profiling could enable the distinction between SGD and MGD. The comparison between IOPTH and HRMAS NMR could be of particular interest in patients with concordant imaging results but also in cases of doubtful or discordant imaging findings. HRMAS NMR also provides new insights into the relationships between metabolic pathways and parathyroid disorders.

In the setting of PHPT, we have found that SGDs (all adenomas) exhibit a higher concentration of myo-inositol, scyllo-inositol, choline, phosphorylcholine, and glycerophosphocholine than hyperplastic glands. These metabolites belong to the structural components of cell membranes.²⁹ Myoinositol is the precursor of phosphatidylinositol, a constituent of phospholipid membranes, and is involved in cell signaling.³⁰ Interestingly, recent studies have shown that ¹⁸F-fluorocholine positron emission tomography (PET) is a very promising imaging method for localization of parathyroid adenomas.³¹⁻³⁶

Our results are in agreement with these observations and could represent the biologic substrate and justification to the use of ¹⁸F-fluorocholine PET imaging in HPT. Moreover, a higher amount of succinate and fumarate was shown by network analysis within SGD compared with MGD, suggesting an increased activity of the tricarboxylic acid cycle. By contrast, MGDs exhibit a higher level of glutamate, GSH, and ascorbate, which act as antioxidants. Hyperplastic glands from PHPT also have higher levels of GSH, aspartate, and glutamate compared with those from renal HPT.

We acknowledge some limitations to the present study. First, there are a limited number of patients included in our study as well as a limited number of analyzed samples. We believe these data are preliminary and should be validated in further series. Second, patients with PHPT and MGD may have multiple adenomas in 5–7% of cases. This subset of patients is considered to be difficult to diagnose using intraoperative PTH, but this difficulty may be similar when using HRMAS NMR spectroscopy.

However, included patients with MGD did not have multiple adenomas, which might have led us to wrong conclusions about this study. Third, we acknowledge that a comparative-effectiveness study should be performed in real time to evaluate IOPTH versus HRMAS NMR spectroscopy before drawing any definitive conclusions. Lastly, this study was retrospective and may involve some bias that would have been unaccounted for.

In conclusion, the present study shows that HRMAS NMR spectroscopy provides unique and accurate information in the metabolomic classification of hyperfunctioning parathyroid glands. Furthermore, this could deepen our knowledge of hyperparathyroidism pathogenesis and may also lead to the identification of new targets for diagnosis, imaging, or future therapeutic options. Finally, if these results are confirmed in further studies, it is expected that the role of intraoperative HRMAS NMR spectroscopy could then be evaluated in the setting of PHPT.

REFERENCES

1. Bilezikian JP, Brandi ML, Eastell R, Silverberg SJ, Udelsman, et al. Guidelines for the Management of Asymptomatic Primary Hyperparathyroidism: Summary Statement from the Fourth International Workshop. *J Clin Endocrinol Metab* 2014;99:3561-9.
2. Guerin C, Lowery A, Gabriel S, Castinetti F, Philippon M, Vaillant-Lombard J, et al. Preoperative imaging for focused parathyroidectomy: Making a good strategy even. *Eur J Endocrinol* 2015;172:519-26.
3. Ritchie SA, Ahiahonu PW, Jayasinghe D, Heath D, Liu J, Lu Y, et al. Reduced levels of hydroxylated, polyunsaturated ultra long-chain fatty acids in the serum of colorectal cancer patients: Implications for early screening and detection. *BMC Med* 2010;8:13.
4. Denkert C, Buche E, Hilvo M, Salek R, Oresic M, Griffin J, et al. Metabolomics of human breast cancer: New approaches for tumor typing and biomarker discovery. *Genome Med* 2012;4:37.
5. Duarte IF, Stanley EG, Holmes E, Lindon JC, Gil AM, Tang H, et al. Metabolic assessment of human liver transplants from biopsy samples at the donor and recipient stages using high-resolution magic angle spinning 1H NMR spectroscopy. *Anal Chem* 2005;77:5570-8.

6. Ritchie SA, Akita I, Takemasa I, Eguchi H, Pastural E, Nagano H, et al. Metabolic system alterations in pancreatic cancer patient serum: Potential for early detection. *BMC Cancer* 2013;13:413.
7. Griffin JL, Shocker JP. Metabolic profiles of cancer cells. *Nature Reviews. Cancer* 2004;4:551-61.
8. Imperiale A, Moussalieh FM, Roche P, Battini S, Cicek AE, Sebag F, et al. Metabolome profiling by HRMAS NMR spectroscopy of pheochromocytomas and paragangliomas detects SDH deficiency: Clinical and pathophysiological implications. *Neoplasia* 2014;17:55-65.
9. Imperiale A, Moussalieh FM, Sebag F, Brunaud L, Barlier A, Elbayed K, et al. A new specific succinate-glutamate metabolomic hallmark in sdhx-related paragangliomas. *PLoS One* 2013;8:e80539.
10. Piotta M, Moussalieh FM, Imperiale A, Benahmed MA, Detour J, Bellocq JP, et al. Reproducible sample preparation and spectrum acquisition techniques for metabolic profiling of human tissues by proton high-resolution magic angle spinning nuclear magnetic resonance. In: Lutz P, editor. *Methodologies for metabolomics. Experimental strategies and techniques*. Cambridge (UK): Cambridge University Press; 2012. p. 496-524.
11. Wishart DS, Jewison T, Guo AC, Wilson M, Knox C, Liu Y, et al. HMDB 3.0—The human metabolome database. *Nucleic Acids Res* 2013;41:D801-7.
12. Seierstad T, Roe K, Sitter B, Halgunset J, Flatmark K, Ree AH, et al. Principal component analysis for the comparison of metabolic profiles from human. *Mol Cancer* 2008; 25:7-33.
13. Wold S, Albano C, Dunn W III, Edlund U, Esbensen K, Geladi P, et al. Multivariate data analysis in chemistry. In: Kowalski BR, editor. *Chemometrics: Mathematics and statistics in chemistry*. Dordrecht (The Netherlands): Reidel; 1984. p. 17-95.
14. Chong IG, Jun CH. Performance of some variable selection methods when multicollinearity is present. *Chemolab* 2005; 78:103-12.
15. Picard RR, Cook RD. Cross-validation of regression models. *J Am Stat Assoc* 1984;79:575-83.
16. Wold S, Ruhe A, Wold H, Dunn WJ. The collinearity problem in linear regression - the partial least-squares (PLS) approach to generalized inverses. *SIAM J Sci Stat Comput* 1984;5:735-43.
17. Cicek AE, Bederman I, Henderson L, Drumm ML, Ozsoyoglu G. ADEMA: An algorithm to determine expected metabolite level alterations using mutual information. *PLoS Comput Biol* 2013;9:e1002859.
18. Kanehisa M, Goto S. KEGG: Kyoto encyclopedia of genes and genomes. *Nucleic Acids Res* 2000;28:27-30.
19. Kanehisa M, Goto S, Sato Y, Kawashima M, Furumichi M, Tanabe M. Data, information, knowledge and principle: Back to metabolism in KEGG. *Nucleic Acids Res* 2014;42: D199-205.
20. Selway ZZ. *Metabolism at a glance*. 3rd ed. Malden (MI): Blackwell Publishing; 2014.
21. Greene AB, Butler RS, McIntyre S, Barbosa GF, Mitchell J, Berber E, et al. National trends in parathyroid surgery from 1998 to 2008: A decade of change. *J Am Coll Surg* 2009;209:332-43.
22. Kunstman JW, Kirsch JD, Mahajan A, Udelsman R. Clinical review: Parathyroid localization and implications for clinical management. *J Clin Endocrinol Metab* 2013;98: 902-12.
23. Udelsman R, Akerstrom G, Biagini C, Duh QY, Miccoli P, Niederle B, et al. The surgical management of asymptomatic primary hyperparathyroidism: Proceedings of the fourth international workshop. *J Clin Endocrinol Metab* 2014;99:3595-606.
24. Molinari AS, Irvin GL 3rd, Deriso GT, Bott L. Incidence of multiglandular disease in primary hyperparathyroidism determined by parathyroid hormone secretion. *Surgery* 1996;120:934-7.
25. Gauger PG, Agarwal G, England BG, Delbridge LW, Matz KA, Wilkinson M, et al. Intraoperative parathyroid hormone monitoring fails to detect double parathyroid adenomas: A 2-institution experience. *Surgery* 2001;130: 1005-10.
26. Miller BS, England BG, Nehs M, Burney RE, Doherty GM, Gauger PG. Interpretation of intraoperative parathyroid hormone monitoring in patients with baseline parathyroid hormone levels of <100 pg/mL. *Surgery* 2006;140:883-90.
27. Siperstein A, Berber E, Barbosa GF, Tsinberg M, Greene AB, Mitchell J, et al. Predicting the success of limited exploration for primary hyperparathyroidism using ultrasound, sestamibi, and intraoperative parathyroid hormone: Analysis of 1,158 cases. *Ann Surg* 2008;248:420-8.
28. Weber CJ, Ritchie JC. Retrospective analysis of sequential changes in serum intact parathyroid hormone levels during conventional parathyroid exploration. *Surgery* 1999;126: 1139-43.
29. Kreis R, Ross BD, Farrow NA, Ackerman Z. Metabolic disorders of the brain in chronic hepatic encephalopathy detected with H-1 NMR spectroscopy. *Radiology* 1992;182: 19-27.
30. Berridge MJ, Downes CP, Harley MR. Neural and developmental actions of lithium: A unifying hypothesis. *Cell* 1989; 59:411-9.
31. Lezaic L, Rep S, Sever MJ, Kocjan T, Hocevar M, Fettich J. 18F-Fluorocholine PET/CT for localization of hyperfunctioning parathyroid tissue in primary hyperparathyroidism: A pilot study. *Eur J Nucl Med Mol Imaging* 2014;41:2083-9.
32. Hindie E, Zanotti-Fregonara P, Tabarin A, Rubello D, Morelec I, Wagner T, et al. The role of radionuclide imaging in the surgical management of primary hyperparathyroidism. *J Nucl Med* 2015;56:737-44.
33. Michaud L, Burgess A, Huchet V, Lefèvre M, Tassard M, Ohnona J, et al. Is 18F-fluorocholine-positron emission tomography/computerized tomography a new imaging tool for detecting hyperfunctioning parathyroid glands in primary or secondary hyperparathyroidism? *J Clin Endocrinol Metab* 2014;99:4531-6.
34. Kluijfhout WP, Vorselaars WM, Vriens MR, Borel Rinkes IH, Valk GD, de Keizer B. Enabling minimal invasive parathyroidectomy for patients with primary hyperparathyroidism using Tc-99m-sestamibi SPECT-CT, ultrasound and first results of 18F-fluorocholine PET-CT. *Eur J Radiol* 2015;84: 1745-51.
35. Paul A, Villepelet A, Lefèvre M, Périé S. Oncocytic parathyroid adenoma. *Eur Ann Otorhinolaryngol Head Neck Dis* 2015;132:301-3.
36. Michaud L, Balogova S, Burgess A, Ohnona J, Huchet V, Kerrou K, et al. A pilot comparison of 18F-fluorocholine PET/CT, ultrasonography and 123I/99mTc-sestaMIBI dual-phase dual-isotope scintigraphy in the preoperative localization of hyperfunctioning parathyroid glands in primary or secondary hyperparathyroidism: Influence of thyroid anomalies. *Medicine* 2015;94:e1701.